SST forcings and Sahel rainfall variability in simulations of the 20^{th} and 21^{st} centuries.

M. Biasutti [1] I. M. Held [2] A. H. Sobel [3] A. Giannini [4]

Received _____; accepted _____

Revised for Journal of Climate,

Corresponding author address: Michela Biasutti, Lamont-Doherty Earth Observatory of Columbia University - Oceanography

61 Route 9W - PO Box 1000, Palisades, NY 10968-8000.

E-mail: biasutti@ldeo.columbia.edu

Short title:

[1]Lamont-Doherty Earth Observatory of Columbia University, Palisades, NY.

[2]Geophysical Fluid Dynamics Laboratory/ NOAA, Princeton, NJ.

[3]Columbia University, New York, NY.

[4]International Research Institute for Climate and Society, Palisades, NY.

ABSTRACT

The outlook for Sahel precipitation in coupled simulations of the 21st century is very uncertain, with different models disagreeing even on the sign of the trends. Such disagreement is especially surprising in light of the robust response of the same coupled models to the 20th century forcings.

We present a statistical analysis of the pre-industrial, 20th century and 21st century A1B scenario simulations among the latest Coupled Model Intercomparison Project dataset (CMIP3). We show that the relationship that links Sahel rainfall anomalies to tropical sea surface temperature (SST) anomalies at interannual time scales in observations is reproduced by most models, independently of the change in the basic state as the world warms.

The same SST/Sahel relationship can be used to predict the simulated 20th century changes in Sahel rainfall from each model's simulation of changes in Indo-Pacific SST and Atlantic SST meridional gradient, although the prediction overestimates the simulated trends. Conversely, such a relationship does not explain the rainfall trend in the 21st century in a majority of models. These results are consistent with there being, in most models, a substantial direct positive effect of atmospheric greenhouse gases on Sahel rainfall, not mediated through SST.

1. Introduction

During the second half of the 20th century Africa witnessed one of the most remarkable climate signals of the recent observational record in the pronounced negative trend in rainfall in the semi-arid Sahel, the southern edge of the Sahara desert, which culminated in the devastating drought of 1984 (e.g. Nicholson, 1980; Nicholson et al., 2000).

Given the large environmental and human impact of drought in this region, it is important to understand whether the drought of the 1970s and 1980s was a consequence of global warming and a harbinger of worse things to come, as many outside the scholarly community have already suggested (e.g., Gore, 2006), or whether the past drought was caused by other factors and the most recent upswing in rainfall (Nicholson et al., 2000) is the beginning of a steady recovery.

Our understanding of the Sahel drought has been growing thanks to many modeling studies that have employed both uncoupled and coupled general circulation models (GCMs). Recently, different atmospheric GCMs (Folland et al., 1986; Giannini et al., 2003; Tippett and Giannini, 2006; Lu and Delworth, 2005; Hoerling et al., 2006) forced with the historic timeseries of global sea surface temperature (SST), have been able to reproduce the main outlines of the 20th century Sahel pluvials and droughts, thus demonstrating that oceanic forcing has been the dominant driver of rainfall variability in this region. It appears that land surface and vegetation processes and perhaps dust feedbacks may amplify rainfall anomalies, but do not in themselves create realistic anomalies in the absence of these SST variations (e.g., Zeng et al., 1999; Giannini et al., 2003; Rosenfeld et al., 2001).

Other modeling studies have tackled the question of whether one should attribute the 20th century Sahel droughts to internal climate variability or to anthropogenic emissions of greenhouse gases and aerosols. Rotstayn and Lohmann (2002) and Hoerling

et al. (2006), following Folland et al. (1986) and others, have both emphasized the role of the differential warming of the northern and southern hemispheres in determining the meridional location of the Atlantic ITCZ and the reach of the west African monsoon. Yet the former study argued for the role of anthropogenic aerosol in forcing Sahel drought, while the latter argued for natural variability. Giannini et al. (2003, 2005) and Bader and Latif (2003) have emphasized the warming of the tropical oceans, especially the Indian Ocean, as a possible cause of drying of the Sahel. Such a warming has been linked by Stott et al. (2000) and Knutson et al. (1999), among others, to anthropogenic greenhouse gases.

Biasutti and Giannini (2006) took advantage of the third Coupled Model Intercomparison Project (CMIP3) dataset and looked at Sahel rainfall variations in 19 different coupled GCMs. Most models (16 out of 19) simulate a significantly drier Sahel at the end of the 20$^{\text{th}}$ century with respect to the pre-industrial times. At least 30% of the observed negative rainfall trend over the 1930-2000 period was estimated to be externally—and most likely anthropogenically—forced. They concluded that, while the role of internal climate variability was predominant in forcing the sharp decline in Sahel rainfall of the 1960s and 1970s, anthropogenic influences have also been substantial, giving reasons to worry about the future.

In simulations in which greenhouse gases are the only or dominant forcing, the agreement seen in the late 20$^{\text{th}}$ century response breaks down (Held et al., 2005; Biasutti and Giannini, 2006; Cook and Vizy, 2006; Lau et al., 2006). The fact that the 20$^{\text{th}}$ century drying does not continue in the 21$^{\text{st}}$ century in a majority of models would suggest that aerosols, and not greenhouse gases, have forced drought on the Sahel in these models of the 20$^{\text{th}}$ century.

Biasutti and Giannini (2006) attribute the cross-model consensus in the 20$^{\text{th}}$ century integrations to the fact that models respond in a consistent fashion to the

cross-equatorial gradient of SST forced by reflective aerosols and Hoerling et al. (2006) point to the reversal in the Atlantic SST gradient as the global warming signal intensifies and aerosols go away as the cause of a predicted recovery in Sahel rainfall. Yet, Held et al. (2005) find that the coupled models of the Geophysical Fluid Dynamics Laboratory (GFDL) respond to increasing greenhouse gases with a very robust drying in the Sahel, even in the presence of a reversal of the Atlantic gradient. Moreover, simulations with some uncoupled atmospheric models do indicate a drying of the Sahel in response to either a uniform warming or a warming of the Indian ocean (Held et al., 2005; Bader and Latif, 2003), which indicates that drying is a plausible response to increased greenhouse gas concentrations.

Our understanding of the processes governing tropical rainfall is insufficient to predict with certainty a trend of either sign: Enhanced precipitation in the monsoons would be expected as a consequence of the enhanced land/sea temperature contrast typical of the global warming signal (Haarsma et al., 2005). On the other hand, regions where moisture availability is limited by dry advection (such as the Sahel, which lies downwind from the Sahara) might dry in the future if they do not reach the new threshold in boundary layer moist static energy necessary for deep convection in a warmer, more stable environment (Neelin et al., 2003). Thus, as pointed out by several studies (Held et al., 2005; Cook and Vizy, 2006; Lau et al., 2006; Biasutti and Giannini, 2006) and exemplified by Figure 1, the outlook for rainfall in the Sahel is very uncertain: we do not know whether we should expect positive or negative rainfall anomalies in the Sahel under global warming.

We are interested in understanding how such disparate predictions for the future of Sahel rainfall come about in different models. One possibility is that different models have different sensitivities to local and remote SST forcings of rainfall over the Sahel. For example, a warmer north Atlantic ocean could enhance the southerly flow and hence

the moisture flux into the Sahel and could lead to more rain. A warmer Indo-Pacific ocean could warm and stabilize the tropical troposphere and, in analogy to a warm ENSO event, lead to a dryer Sahel. If different models weigh these processes differently, their outlooks for Sahel rainfall will differ as well. Another possibility is that the models predict patterns of SST anomalies for the 21st century that are different enough to force different Sahel responses, even if the sensitivities in each model are quite similar. Moreover, other forcings besides SST can become more important in the future: for example, land surface temperatures are expected to rise faster than SSTs (e.g. Houghton et al., 1995; Sutton et al., 2007), leading to an enhanced land-sea contrast and, possibly, monsoon rainfall (Haarsma et al., 2005). Again, models might differ in how strong a land-sea contrast they predict or in how sensitive they are to this mechanism.

We focus on the role of changing SST in forcing changes in Sahel rainfall. We analyze the pre-industrial control integrations, the 20th century integrations and the 21st century A1B scenario integrations of 19 among the CMIP3 models. We estimate the sensitivity of Sahel rainfall to local and remote SST forcings by looking at the strength of the statistical relationship between the Sahel rainfall index and the relevant quantities; and we address the question of whether it is possible to predict the 21st century response of a model to tropical SST changes from knowledge of its behavior in the 20th century.

In Section 2 we describe the integrations in more detail, introduce the models and assess their overall performance in simulating Sahel rainfall variability. In Section 3 we report on the statistical relationship between Sahel rainfall and SST, as simulated by the models in the pre-industrial and 20th century integrations. In Section 4 we investigate whether the relationships that have emerged at interannual timescales and in the forced changes of the 20th century are relevant for the 21st century trend. In Section 5 we offer our conclusions.

2. Datasets

Our dataset is extracted from the third Coupled Model Intercomparison Project (CMIP3) dataset, which we obtained from the Program for Climate Model Diagnosis and Intercomparison (PCMDI) website. We have analyzed the 20th Century (hereafter XX), pre-industrial control (hereafter PI), and A1B scenario integrations (hereafter A1B) of nineteen coupled models. In the XX simulations, the coupled models are forced by the historic,varying concentrations of well-mixed greenhouse gases and sulfate aerosols, and—in some models—by other anthropogenic (e.g., black carbon particulate, or land use patterns) and natural (solar output and volcanic aerosols) forcings. The PI controls have constant forcings, with CO_2 and aerosol concentrations held at the pre-industrial level. The A1B scenario assumes a growing world economy and technological advances, such that the concentration of CO_2 reaches 700ppmv in 2100 and stabilizes at that level, while aerosol concentration decreases. In most of our analyses we have used the entire length of the XX simulations, 200 years (when available) of the PI simulations, and the first 100 years of the A1B simulations. Table 1 provides a brief overview of the characteristics of the models and the simulations. A full description of all models and integrations can be found at www-pcmdi.llnl.gov/ipcc/model_documentation/ipcc_model_documentation.php and references therein.

Our choice of models was dictated exclusively by the availability of the integrations when we recovered the data: we included all the available models, independently of the characteristics of their simulation over Africa. While it is likely that the 21st century simulation of Sahel rainfall can be compromised by a model's inability to reproduce the observed climatology or the observed relationship between Sahel rainfall and global SSTs for the present and recent past, we do not know a priori what model characteristics are important in determining the 21st century response.

Figure 2 contrasts the annual cycle of rainfall averaged over 10°N-20°N across Africa in two observational datasets that cover a drier and a wetter period (CMAP (Xie and Arkin, 1996, 1997), covering 1979-1999, and Hulme (Hulme, 1992), covering 1900-1998) and in the models (for each model we show the climatology in the PI, XX, and A1B integrations). There is a large spread across models in the amount of precipitation falling on the Sahel, with a tendency to underestimate it, sometimes dramatically (as for the IPSL model). All of the models at least capture the gross features of the mean seasonal cycle of Sahel rainfall, with maximum precipitation in the summer months, although some tend to simulate a faster increase of precipitation in the spring (for example the UKMO HADCM3), others a slower decline in the fall (e.g., CNRM CM3). The shape of the seasonal cycle is not appreciably or consistently changed across the PI, XX and A1B simulations, and thus results in the rest of the paper are only shown for the northern monsoon season, defined as July, August, September (JAS).

In Figure 3 we explore the spatial characteristics of rainfall in the region. The contour lines show the mean position of summer rainfall over Africa and the Atlantic basin in observations and the coupled models. In observations (CMAP, Figure 3.xx), the maximum JAS precipitation extends over Africa from the equator to about 18N and is concentrated over the ocean in the Atlantic ITCZ, stretching from West Africa across the basin, at about 8N. Precipitation is more intense in the ITCZ than over the continent. The models show some fairly common biases. Over Africa, rain in many models does not extend far enough north; over the ocean, the ITCZ is often positioned too far south and widens over the Gulf of Guinea. This bias is linked to most models' inability to develop a cold tongue in the Gulf of Guinea (see Davey et al., 2002).

Given that, in these models, the climatologies are far from perfect, and in particular that often the rainband stays shy of the Sahel, a single index defined on the basis of observations might not be optimal to capture the variability in this region. We

have elected not to correct for individual model bias, and we define as Sahel index the JAS rainfall in the 10°N-20°N zonal band over Africa. To provide a measure of how well the pattern of Sahel rainfall variability is captured by this index, we calculate its correlation with global rainfall in each PI integration (Figure 3, shading). In observations (Fig. 3.xx), correlations are—as expected—strong and positive in the region used to define the Sahel index, but they are quite noisy elsewhere (this might in part be due to the shortness of the CMAP record). There is a signature of the dipole between the Sahel and the Gulf of Guinea, and of some positive correlation with rainfall at the northern edge of the ITCZ, although it is limited to a region near the coast. Overall, this Sahel index, which is based on observations, does capture the local rainfall variability in the coupled models, but the correlation patterns of Fig. 3 are affected by the biases in the models' rainfall climatology. In some models the pattern is too narrow (e.g. Fig. 3.xv), in others too wide (e.g. Figs. 3.viii and 3.xviii), in others not zonal enough (e.g. Fig. 3.ii), in others weak enough to suggest little coherence across the Sahel (e.g. Figs 3.iii and 3.xvi). The correlations between the Sahel and oceanic precipitation also vary widely across models, with some models emphasizing the connection to the northern edge of the ITCZ (e.g. Fig. 3.xviii) and other emphasizing the dipole with Guinea (e.g. Fig. 3.xiii). In the remainder of this paper we will present results for the Sahel index as defined above, with the understanding that a few of the models do not accurately capture its mean magnitude, nor the associated spatial pattern of interannual variability. Two examples of the behavior of the simulated Sahel rainfall index in the XX and A1B integrations were given in Figure 1.

3. Relationship between SST and Sahel rainfall in the PI and XX Integrations.

As many studies with atmospheric GCMs and prescribed SST have demonstrated, the Sahel droughts and pluvials recorded in the observational record were largely forced by SST. Thus, we begin this section investigating how the models reproduce the statistical relationship between Sahel rainfall and global SST. In this section we focus on the characteristics of the natural variability and the 20^{th} century trend.

Figure 4a displays a measure of the cross-model agreement in reproducing the linear correlation between the summer Sahel rainfall index and global surface air temperature at interannual-to-interdecadal timescales during pre-industrial times (for ocean regions, surface air temperature and SST are so tightly linked that we will use the two terms interchangeably). The figure is constructed in the following way. First, we calculate the correlation between the detrended Sahel rainfall and surface temperature time series for each of the 19 PI integrations (detrending should not be necessary, but some of the PI integrations experience climate drift); second, at every gridpoint we assign a value of +1 if the correlation is significant at the 95% level and positive, and -1 if it is significant and negative (significance is calculated assuming that each year is an independent sample); third, we take the sum over all 19 models, and plot it as a percentage.

There is a strong agreement across models on the fact that increased precipitation over the Sahel coexists with a locally cooler surface temperature, most likely because rain leads to cooling through increased surface evaporation and the associated cloudiness leads to a reduction of short-wave input. The positive Sahel correlation with surface temperature in the eastern Sahara and northern Arabian Peninsula is also very robust. Conversely, the relationship between Sahel rainfall and global SST is weaker, according to this metric. For example, there is only a 50% agreement that the Sahel index is significantly negatively correlated with SST in the tropical Pacific, and the agreement

drops further in the eastern equatorial Pacific, where the ENSO signal, even in summer, should be strongest. When we repeat this calculation on a 5-year running mean, the agreement in the ENSO region becomes greater, suggesting some sensitivity to the details of the SST pattern (see also the discussion of Figure 6 below). The agreement on the anticorrelation with the south tropical Atlantic exceeds 60%; the correlation pattern in the north tropical Atlantic is weaker and somewhat noisy.

What emerges in Figure 4a is an overall inter-model agreement on the large scale pattern of correlation: the models indicate that at interannual-to-interdecadal time scales, a wet (dry) Sahel tends to be associated with cooler (warmer) tropics and a positive (negative) SST gradient across the tropical Atlantic. This pattern is quite similar to that seen in observations (Figure 5, Folland et al., 1986; Giannini et al., 2005), although the features of the SST pattern that have been deemed more relevant to explain the 20th century variability in observations are not necessarily the more robust across the models. In particular, Giannini et al. (2005) stress the importance of the Indian Ocean warming in forcing drought over the Sahel during the later part of the 20th century, but the PI runs do not reproduce high correlation in this region. A possible explanation is that the relationship between the Indian Ocean and the Sahel is most apparent at the time scale of the forced trend, and is muted when natural variability at shorter time scales is considered. We note that the positive correlation of Sahel rainfall with mid-latitude surface temperature is significant in the models but not in observations (Giannini et al., 2005), maybe due to the smaller signal to noise ratio of variability in the mid-latitudes, compared to the tropics.

The relationship with SST that characterizes the interannual-to-interdecadal variability in Sahel rainfall is robust across different epochs, according to the IPCC models. Figure 4b (built as Figure 4a and showing the across-model agreement over significant correlation) shows that the pattern of correlation between the detrended time

series of SST and Sahel rainfall in the XX simulations is very similar to that in the PI case. The same result also holds for the global warming integrations A1B (see Figure 9 in the next section). We conclude that the interannual-to-interdecadal relationship between Sahel rainfall and global surface temperature patterns is left unchanged in its broader features as the basic state changes under the effect of anthropogenic forcings.

To focus on the large scale pattern that has emerged in Figure 4, instead of looking at gridpoint-by-gridpoint agreement, and in order to consider each model individually, we now assess the relationship between Sahel rainfall and two indices of large-scale SST variability. We choose the SST indices based on Figure 4 and the body of literature regarding the relationship between Sahel rainfall and SST. First of all, we limit our indices to the Tropical SST, which is the main driver of tropical rainfall changes. One index is the mean Indo-Pacific SST; this broad-scale index emphasizes time scales longer than the interannual ENSO time scale and also captures the variability of the Indian Ocean that has been implicated in the long-term drought of the Sahel in the 20$^{\text{th}}$ century (see for example Giannini et al., 2003, for the influence of ENSO and Indian Ocean SST on Sahel rainfall at different time scales). The second index is the North-South SST gradient in the tropical Atlantic. The studies that viewed the Sahel drought as part of a shift in the meridional position of the ITCZ have emphasized the role of either the local, Atlantic SST (e.g., Cook and Vizy, 2006) or a global, interhemispheric gradient (e.g., Folland et al., 1986); we choose to focus on the local SST gradient because we do not see in Figure 4 any evidence of inter-hemispheric antisymmetry in the pattern of correlation to SST: to the contrary, we see a high degree of symmetry in the two hemispheres, with negative correlation in the tropics and positive correlation poleward, only weakly disrupted in the north tropical Atlantic by a patch of positive correlations below 20°N and along the African coast.

Other choices of indices were also possible. We have repeated our analysis using

three SST indices (the tropical Atlantic, the Atlantic meridional gradient, and either the Indo-Pacific or the Pacific) so to better capture both the meridional and the zonal gradients of tropical SST, and find no significant differences in our results.

To focus on the Sahel/SST relationship that emerges from natural variability, we analyze the PI integrations. We calculate the box average SST in the tropical Indo-Pacific (20°S-20°N; 50°E-90°W) and a bulk tropical Atlantic SST meridional gradient [north (7°N-30°N; 70°W-20°W) minus south (20°S-7°N; 40°W-5°E)] and calculate the correlation of these coarser indicators of patterns of SST anomalies with the Sahel index. Figure 6 shows that there is a much stronger model agreement according to this metric than in the case of gridpoint-by-gridpoint comparison. Correlations are more consistent and stronger when we filter out the fastest interannual variability with a 5-year running mean, so we discuss this case. Thirteen out of nineteen models have a significant (at the 95% level, shown in Figure 6 by the grey shading) negative correlation between the Sahel index and Indo-Pacific SST (two models show significant positive correlations), and fifteen models show significant positive correlations with the Atlantic north-south gradient (the rest of the models show insignificant, but still positive, correlations)[1].

The right panels of Figure 6 show the regression coefficients for a bi-variate linear model that uses the Indo-Pacifc SST and the Atlantic SST meridional gradient indices to predict variations in Sahel rainfall. According to this measure, although the relationship

[1]Significance for the 5-year running means is calculated considering one degree of freedom every 5 points. Correlations with single basins are somewhat less robust than with the Indo-Pacific and Atlantic gradient indices: correlations with the Pacific and South Atlantic indices resemble those to the Indo-Pacific and Atlantic gradient, respectively, but correlations with the North Atlantic change sign in different models, confirming the weaker relationship seen in Figure 4.

between the Sahel and the Atlantic is more robust, the relationship with the Indo-Pacific is more influential: the regression coefficients for the Indo-Pacific are about twice as large as those for the Atlantic.

A rough estimate of how much (5-year running mean) Sahel rainfall variability is forced by SSTs in these coupled integrations can be obtained by comparing the prediction of the simple bi-variate regression and the coupled models' Sahel rainfall variations.

Figure 7a shows the correlation between the linearly predicted Sahel index and the original, simulated Sahel index in the integrations used to train the regression model (that is, the PI integrations). As expected, all models show positive correlations, and 13 show correlations better than 0.4. The fraction of variance in Sahel rainfall explained by SST is not large, but this is to be expected because we are considering only one realization of a coupled integration, and the variability linked to SST is small compared to the total variability. Another possible explanation is that the regression model, while accurate in reproducing multidecadal variability, tends to dampen the variability at shorter timescales (not shown). The spread among models is large: correlations range between about .7 (MRI) to virtually zero (CCSM3), an expected result given the range of Sahel/SST correlations shown in Figure 6.

Can we use the Sahel/SST relationship that we have derived from the natural variability in the PI integrations to interpret the behavior of Sahel rainfall in the presence of external forcings during the 20^{th} and 21^{st} centuries? Here, we address these questions for the XX integrations; the case of the 21^{st} century is explored in the next section.

Figure 7b shows the correlation between the XX simulated Sahel and the predicted Sahel (obtained from the XX SST indices, using the regression coefficients derived from the PI integrations) calculated either for the 5-yr running mean, detrended timeseries

or the 5-yr running mean timeseries (for which only the shortest timescales have been muted, and variance arises at all longer time scales, including the centennial trend, which is largely externally forced, squares). Only one realization of the XX simulations is used for each model. Our simple linear model—derived from the natural variability in pre-industrial times—has some predictive skill for the 20th century, whether we predict the full timeseries or only its shorter-term variability. Correlations between the original and the synthetic Sahel time series are positive in most cases (with the notable exception of the two NCAR and the MPI models), whether or not the centennial trend is included. This would seem to indicate that the trend in 20th century Sahel rainfall arises from the SST trends through the same mechanisms that shape the SST-forced interannual variability. The correlation between the predicted and simulated Sahel rainfall is in general somewhat better when we predict the full timeseries than when we predict only its short-term variability, which is consistent with the expectation that variability at shorter time scales would be affected by atmospheric internal variability more than would the trend.

A direct comparison (Figure 8) of the simulated Sahel 20th century trends with those linearly predicted from the XX SST confirms that the linear model captures the sign and order of magnitude of the simulated trends. In 11 out of 19 models the linear model produces a stronger drying trend than simulated; this could be just by chance, but the fact that the spurious increases of the negative trend are so much larger than any spurious decrease is suggestive of a tendency for the regression model to overestimate the drying trend. This behavior, and the behavior over the 21st century described in the next section, might indicate that there are other influences on Sahel rainfall, distinct from SST and induced directly by the external forcings.

As another test of the robustness of the SST/Sahel rainfall relationship, we perform a similar calculation, using the first half of the XX integrations to build a linear model

for Sahel rainfall and validating the model by predicting Sahel rainfall changes in the second half of the integrations. In this case we retain the trend in all timeseries, so that the forced component of the relationship can be captured by the linear model (to the extent that the forced signal is present in the early part of the 20th century and is not overwhelmed by natural variability at shorter timescales). The linear model shows some skill in a majority of models (not shown) but it is not as accurate as the model derived from the pre-industrial natural variability and it produces negative correlations between the predicted and simulated Sahel rainfall timeseries in 4 of the models during the validation period.

4. Relationship between SST and Sahel rainfall in the A1B Integrations.

The relationship with global SST that characterizes the natural variability of the Sahel is robust across epochs: the large scale pattern of correlation between the Sahel index and surface temperature that emerges from the A1B integrations at interannual-to-interdecadal timescales—when the trend is removed from the Sahel and temperature time-series—is indistinguishable from that of the pre-industrial and 20th century simulations (cf. Figure 9 to Figure 4 in the previous section). When the trend is retained in the time series the models disagree in the relationship between Sahel rainfall and global trends in surface temperature. In a majority of models the surface global warming is accompanied by a positive trend in Sahel rainfall, in some models the warming is accompanied by drying and in others there is no significant correlation.

Figure 10 shows how, in each A1B simulation, the Sahel/SST relationship changes when the centennial trend is kept or removed. Specifically, Figure 10 shows the correlation between the simulated and predicted 21st century Sahel for two linear regression models: the first is the one introduced in the previous section in Figs 6

and 7, the second is similar, but built on the entire XX runs (5-yr running means are applied, trend is retained). In both cases—whether the bi-variate regression model is built on the natural variability in the pre-industrial runs (Figure 10, left) or on the forced 20th century runs (Figure 10, right)—variations in SST capture only the interannual-to-interdecadal variations in Sahel rainfall (i.e. variations in the detrended time series, circles), but not the trend: in a majority of models the correlation between the simulated Sahel and the synthetic, SST-derived Sahel is negative when the trend is retained in the calculations (squares). To test whether the two predictors used for interannual variability were insufficient to capture the important pattern of SST anomalies in the forced 21st case, we also built a linear model using, besides the Indo-Pacifc and the Atlantic gradient, also the tropical Atlantic SST (or, which is the same, using the north and south tropical Atlantic as independent predictors). This way we can better capture the variability of the zonal gradient of tropical SST. Still, the AIB Sahel rainfall could not be captured in many of the models, regardless of whether the model was built from the PI or the XX integrations.

If one wanted to ascribe the disparate projections for 21st century Sahel rainfall to SST, one might consider a few possibilities: one is that the pathways of SST influence are the same across models and epochs, but different models produce different SST anomalies under global warming. Another possibility is that, although the SST anomalies are the same across models, each model weighs the influence of different ocean basins differently, so that a drying influence is dominant in one model, but not in others. A third possibility is that the linear response to SST change that was dominant in driving natural and forced anomalies in Sahel rainfall in the 20th century is not relevant anymore, with new influences arising either from non-linearities or from new patterns of SST anomalies. Finally, ascribing the disparate projections for 21st century Sahel rainfall to SST might not be possible: SST might cease to be the most important

driver for Sahel rainfall change in all the models, and new influences from some other factor in the climate system might become dominant.

The linear regression model presented in Figure 10 accounts for the first two possibilities: it takes into account both differences in trends and in the sensitivities. Thus, to the extent that linear thinking and our choice of SST indices are warranted, we already know that model discrepancies cannot be explained by SST.

To explore this point further, we show (Figure 11) the trend in Sahel rainfall, mean tropical Indo-Pacific SST, tropical Atlantic meridional SST gradient, and three more indices that describe in more detail the pattern of SST or atmospheric circulation changes in the Pacific: the difference in sea level pressure between gridpoints at Tahiti and Darwin, the difference in SST between the West and East Pacific, and the difference between the equatorial and subtropical SST in the Pacific. We have included these indices because they provide some insight on whether a model produces an El-Niño or La Niña like climate change pattern (in the first two cases) or simulates an enhanced equatorial response in the Pacific (a pattern that might better describe the structure of the global warming signal according to Liu et al., 2005). These indices capture details in the Indo-Pacifc anomalies not captured by the mean SST and might indicate changes in the circulation relevant for the Sahel. In all panels in Figure 11 the gray shading indicates the sign of the Sahel trend in each simulation.

As expected, the warming in the Indo-Pacific is a feature of all model simulations, and thus bears no direct relation to discrepancies in the sign of Sahel rainfall anomalies. Changes in the Atlantic gradient, instead, are much more model dependent, with different models producing anomalies of different signs, yet, there is no correspondence between the anomalies in Atlantic gradient and those in Sahel rainfall. For example, the two MIROC models have differently signed anomalies in the gradient, but both produce strong positive anomalies in Sahel rainfall. Conversely, the two GFDL models dry the

Sahel, but not (as already reported by Held et al., 2005) because of a negative trend in the Atlantic gradient. Discrepancies in the sign of the trend for the Pacific indices also fail to match those in Sahel rainfall trend, suggesting that even more refined indices of SST variations would fail to explain the 21st century changes in the Sahel in a consistent way across all models (this has been tested in regression models).

Finally, we present evidence that the sensitivity of Sahel rainfall to SST changes more consistently from one epoch to the next than from one model to another: Figure 12 shows the coefficients of three bi-variate linear regression models for Sahel rainfall that use the Indo-Pacific and Atlantic gradient indices as predictors and are based on the PI, XX, and A1B integrations.

We see that the relationship between the Sahel and the Atlantic gradient is quite consistent across epochs (and thus in the presence or absence of anthropogenic forcings). The relationship with the Indo-Pacific is stronger for many models, but it is more variable and is sensitive to the presence of the trend both in the 20th century (the coefficients maintain the same sign as in the PI integrations in most cases but their magnitude is, in general, much reduced) and especially in the 21st century (the regression coefficients become positive in a majority of models).

This suggests that the negative correlations between the simulated and linearly predicted Sahel in the A1B scenario shown in Figure 10, like those for the latter part of the XX simulations mentioned in the previous section, are a consequence of a changing relationship between the Sahel and the Indo-Pacific warming that becomes evident going from the pre-industrial to the 20th century and from the 20th to the 21st century.

5. Conclusions

The projection for Sahel rainfall changes in response to global warming is highly uncertain, with some coupled models predicting strong dry anomalies, others predicting

strong wet anomalies, and most predicting more modest anomalies of both signs. This disagreement is even more puzzling when compared to the agreement of a vast majority of the CMIP3 models in reproducing a dry Sahel in the late 20th century, compared to the pre-industrial epoch.

Given that previous modeling studies have shown that global SST changes have paced the Sahel droughts and pluvials of the recent history, we have explored the statistical relationship between rainfall and global SST as it is simulated by the CMIP3 models in the pre-industrial (PI), 20th century (XX) and 21st century (A1B). The large scale features of the observed correlation between Sahel rainfall and global SST are reproduced by a majority of models in the context of their natural variability (that is, when we calculate correlations and regressions between detrended timeseries). Sahel rainfall is negatively correlated with the tropical Indo-Pacific SST and positively correlated with the tropical Atlantic meridional SST gradient.

We have used the PI integrations to construct a linear, bi-variate model that predicts Sahel rainfall variations from changes in Indo-Pacific SST and Atlantic SST gradient. This model has some skill in predicting interannual-interdecadal variability in Sahel rainfall in both the XX and A1B integrations. When it is used to predict centennial trends, the model is still useful for the simulations of the 20th century, but fails during the 21st century in a majority of models.

From the above analysis we conclude the following: (i) at interannual time scales, the relationship linking Sahel rainfall to the global SST does not change in any significant or consistent way from the PI, to the XX, to the A1B cases; (ii) the forced component of Sahel rainfall variations during the 20th century can be explained at least in part by the corresponding variations in the Indo-Pacific SST and the Atlantic SST meridional gradient; (iii) the centennial trend that characterizes Sahel rainfall changes in the A1B integration is not explained, for a majority of models, by the same linear

link to SST that explained rainfall variations during pre-industrial times and the 20th century.

In the global warming scenario, the Indo-Pacific warms and there is little trend in the Atlantic gradient. By the mechanisms operating at interannual-to-interdecadal timescales, the Pacific warming would induce a drought in the Sahel, but most models simulate a wetting of the Sahel, hence the negative correlations between the predicted and simulated Sahel. Indeed, there is a very good correspondence between the models for which our "prediction" model fails and those that simulate a wetting of the Sahel in the 21stcentury.

It appears that the future, GHG-forced change in Sahel rainfall is controlled by different mechanisms, not captured by the simple linear relationship that has characterized the past. It may be that the pattern of forced SST anomalies simulated for the 21st century is different enough from the patterns seen at interannual time scales and in the forced response during the 20th century that different pathways of SST influence become dominant. It is possible that small scale features of the tropical SST anomalies not captured in our analysis (which is based on coarse indices) are essential to determine Sahel rainfall changes. Other possibilities are that extratropical SSTs play an important role, or that the assumption of linearity fails.

Alternatively, it may be that SST is not the only player in a warmer world. That a model based on SST variations both overestimates the Sahel drying trend of the 20th century and cannot account for the 21st century moistening of the Sahel predicted by most models is consistent with the following hypothesis: in most models, atmospheric greenhouse gases exert a substantial direct positive effect on Sahel rainfall, not mediated by SST. Further testing is needed to confirm this interpretation of our results.

Another important conclusion that arises from this analysis is that a faithful reproduction of the 20th century is not in itself assurance that any given model will

be accurate in its prediction of the future. More specifically, the fact that two models both dry the Sahel in the 20th century and do so through the same influence of SST anomalies, does not mean that they will behave similarly in a simulation of the future. Therefore, similarity to observations in a simulation of the 20th century climate appears to be a necessary but insufficient condition for a trustworthy prediction of the future.

Acknowledgments. We thank Dr. Jian Lu for many discussions and ideas, the international modeling groups that have produced the datasets here analyzed, the Program for Climate Model Diagnosis and Intercomparison (PCMDI) for serving the CMIP3 data from their website.

The authors acknowledge support from the Earth Institute Cross-Cutting Initiative on Climate-Society Interactions at Columbia University, the David and Lucile Packard Foundation Fellowship in Science and Engineering, and NOAA (grants NA07GP0213, NA06OAR4310143).

REFERENCES

Bader, J. and M. Latif, 2003: The impact of decadal-scale Indian Ocean sea surface temperature anomalies on Sahelian rainfall and the North Atlantic Oscillation. *Geophys. Res. Lett.*, **30**(22), 2169.

Biasutti, M. and A. Giannini, 2006: Robust sahel drying in response to late 20th century forcings. *Geophys. Res. Lett.*, **33**, L11706.

Cook, K. and E. K. Vizy, 2006: Coupled model simulations of the west african monsoon system: 20th and 21st century simulations. *J. Climate*, **19**(15), 3681–3703.

Davey, M., M. Huddleston, K. Sperber, P. Braconnot, F. Bryan, D. Chen, R. Colman, C. Cooper, U. Cubasch, P. Delecluse, D. DeWitt, L. Fairhead, G. Flato, C. Gordon, T. Hogan, M. Ji, M. Kimoto, A. Kitoh, T. Knutson, M. Latif, H. L. Treut, T. Li, S. Manabe, C. Mechoso, G. Meehl, S. Power, E. Roeckner, L. Terray, A. Vintzileos, R. Voss, B. Wang, W. Washington, I. Yoshikawa, J. Yu, S. Yukimoto and S. Zebiak, 2002: STOIC: a study of coupled model climatology and variability in tropical ocean regions. *Clim. Dyn.*, **18**, 403–420.

Folland, C. K., T. N. Palmer and D. Parker, 1986: Sahel rainfall and worldwide sea temperature . *Nature*, **320**, 602–687.

Giannini, A., R. Saravanan and P. Chang, 2003: Oceanic forcing of Sahel rainfall on interannual to interdecadal time scale. *Science*, **302**, 1027–1030.

Giannini, A., R. Saravanan and P. Chang, 2005: Dynamics of the African monsoon in the NSIPP1 atmospheric model. *Clim. Dyn.*, **25**(5), 517–535.

Gore, A., 2006: *An inconvenient truth*. Rodale Press.

Haarsma, R. J., F. M. Selten, S. L. Weber and M. Kliphuis, 2005: Sahel rainfall variability and response to greenhouse warming. *Geophys. Res. Lett.*, **32**, L17702.

Held, I. M., T. L. Delworth, J. Lu, K. L. Findell and T. R. Knutson, 2005: Simulation of Sahel drought in the 20th and 21st centuries. *Proc. Natl. Acad. Sci.*, **102**(50), 17891–17896.

Hoerling, M., J. Hurrell, J. Eischeid and A. Phillips, 2006: Detection and attribution of 20th century northern and southern African rainfall change. *J. Climate*, **19**(16), 3989–4008.

Houghton, J., L. Meira Filho, B. Callender, N. Harris, A. Kattenberg, K. Maskell and Eds., 1995: Climate change 1995: the science of climate change. p. 572pp., contribution of Working Group I to the Second Assessment of the Intergovernmental Panel on Climate Change. Cambridge University Press.

Hulme, M., 1992: A 1951-80 global land precipitation climatology for the evaluation of general circulation models. *Climate Dyn.*, **7**, 57–72.

Knutson, T. R., D. L. Delworth, K. W. Dixon and R. J. Stouffer, 1999: Model assessment of regional temperature trends (1949-1997). *J. Geophys. Res.*, **104**, 30,981–30,996.

Lau, K. M., S. S. P. Shen, K.-M. Kim, and H. Wang, 2006: A multimodel study of the twentieth-century simulations of sahel drought from the 1970s to 1990s. *J. Geophys. Res.*, **111**(D07111).

Liu, Z., S. Vavrus, F. He, N. Wen and Y. Zhong, 2005: Rethinking tropical ocean response to global warming: The enhanced equatorial warming. *J. Climate*, **18**, 4684–4700.

Lu, J. and T. Delworth, 2005: Oceanic forcing of the late 20th century Sahel drought. *Geophys. Res. Lett.*, **32**, L22706, doi:10.1029/2005GL023316.

Neelin, J. D., C. Chou and H. Su, 2003: Tropical drought regions in global warming and El Nino teleconnections. *Geophys. Res. Lett.*, **30**(24), 2275.

Nicholson, S. E., 1980: The nature of rainfall fluctuations in subtropical West Africa. *Mon. Wea. Rev.*, **108**, 473–487.

Nicholson, S. E., B. Some and B. Kone, 2000: An analysis of recent rainfall conditions in West Africa, including the rainy seasons of the 1997 El Niño and the 1998 La Niña years. *J. Climate*, **13**, 2628–2640.

Rosenfeld, D., Y. Rudich and R. Lahav, 2001: Desert dust suppressing precipitation: A possible desertification feedback loop. *Proc. Natl. Acad. Sci.*, **98**(11), 5975–5980.

Rotstayn, L. D. and U. Lohmann, 2002: Tropical rainfall trends and the indirect aerosol effect. *J. Climate*, **15**, 2103–2116.

Stott, P. A., S. B. F. Tett, G. S. Jones, M. R. Allen, J. F. B. Mitchell and G. J. Jenkins, 2000: External control of 20th century temperature by natural and anthropogenic forcings. *Science*, **290**, 2133–21–36.

Sutton, R. T., B. Dong and J. M. Gregory, 2007: Land/sea warming ratio in response to climate change: Ipcc ar4 model results and comparison with observations,. *Geophys. Res. Lett.*, **34**(L02701).

Tippett, M. and A. Giannini, 2006: Potentially predictable components of African summer rainfall in a SST-forced GCM simulation. *J. Climate*, **19**(13), 3133–3144.

Xie, P. and P. A. Arkin, 1996: Analyses of global monthly precipitation using gauge observations, satellite estimates, and numerical model predictions. *J. Climate*, **9**, 840–858.

Xie, P. and P. A. Arkin, 1997: Global precipitation: a 17-year monthly analysis based on gauge observations, satellite estimates, and numerical model outputs. *Bull. Amer. Meteor. Soc.*, **78**, 2539–2558.

Zeng, N., J. D. Neelin, K.-M. Lau and C. J. Tucker, 1999: Enhancement of interdecadal climate variability in the Sahel by vegetation interaction. *Science*, **286**, 1537–1540.

This manuscript was prepared with AGU's LaTeX macros v3.0, with the extension package 'AGU^{++}' by P. W. Daly, version ? from ?.

Figure Captions

Figure 1. The Sahel rainfall index during the 20^{th} and 21^{st} centuries, as simulated by the GFDL (solid line) and MIROC (dashed line) models. Anomalies are in millimeters per day.

Figure 2. Annual cycle of Sahel precipitation (in mm day^{-1}) in observations (the solid black curve is the mean climatology in the Hulme dataset, the dashed black curve is CMAP) and in simulation of the pre-industrial epoch (PI, red circles), the 20^{th} century (XX, blue squares), and the 21^{st} century (A1B, green asterisks).

Figure 3. Contours: 4 and 8 mm/day contours of JAS precipitation. Shading: Correlation between the Sahel index and JAS rainfall. Warm colors indicate positive correlations, cold colors negative correlations, the shading interval is .08

Figure 4. Percentage of models showing positive (dark grays / warm colors shading, white contours) or negative (light grays / cool colors shading, black contour) significant correlations between the Sahel index and surface temperature at each gridpoint. The left panel is for the PI detrended simulations, the right panel for the XX detrended simulations. The contour interval is 20%, the shading interval 40% (black and white version) or 10% (color version). See text for further details.

Figure 5. Observed positive (dark grays / warm colors shading, white contours) or negative (light grays / cool colors shading, black contour) correlations between the Sahel index (Hulme data set) and sea surface temperature (Kaplan data set) at each gridpoint. The contour interval is 0.20, the shading interval 0.4 (black and white version) or 0.1 (color version).

Figure 6. Pre-industrial correlations (left) and regression coefficients (right) between the Sahel index and (top) the area averaged Indo-Pacific SST and (bottom) the difference of north tropical Atlantic and south tropical Atlantic SST. Open circles are for timeseries that have been detrended; filled circles for detrended and 5-year running mean timeseries.

Figure 7. Correlations between simulated and linearly predicted Sahel index in the (left) PI and (right) XX integrations. The coefficients of the linear model come from the JAS, detrended, 5 year running mean time series of Sahel rainfall, Indo-Pacific SST and Atlantic SST gradient in the PI integrations. All timeseries have been subjected to a 5-yr running mean; dots refer to detrended timeseries, squares to timeseries retaining the trend.

Figure 8. (a.) Linear trends in the simulated XX Sahel rainfall (large squares) and the predicted Sahel timeseries obtained by linear regression from the simulated XX SST (small squares). The linear regression model was trained on the detrended, 5-yr running means of the PI simulations. The trends are calculated over the length of the entire XX simulations, which might cover different periods for different models. (b.) Scatter plot of the simulated and predicted trends shown in panel (a.).

Figure 9. As in Figure 4 but for the A1B simulations.

Figure 10. Correlations between simulated and linearly predicted Sahel index in the A1B integrations. The coefficients of the linear model come from the JAS, 5 year running mean time series of Sahel rainfall, Indo-Pacific SST and Atlantic SST gradient in the (left) detrended PI and (right) XX integrations. All A1B timeseries have been subjected to a 5-yr running mean; dots refer to A1B detrended timeseries, squares to A1B timeseries retaining the trend.

Figure 11. Linear trends over the years 2000-2100 in the A1B integrations in (top left) Sahel index, (middle left) Indo-Pacific SST, (bottom left) Atlantic SST meridional gradient, (top right) Tahiti-Darwin sea level pressure difference, (middle right) west equatorial Pacific - east equatorial Pacific SST difference, and (bottom right) the enhanced equatorial response index (Liu et al., 2005).

Figure 12. Scatter plot of the bi-variate linear model regression coefficients between the Sahel index and the Indo-Pacific SST and Atlantic SST meridional gradient. Red dots are for the PI integrations, blue squares are for XX and green stars are for A1B.

Figure Captions

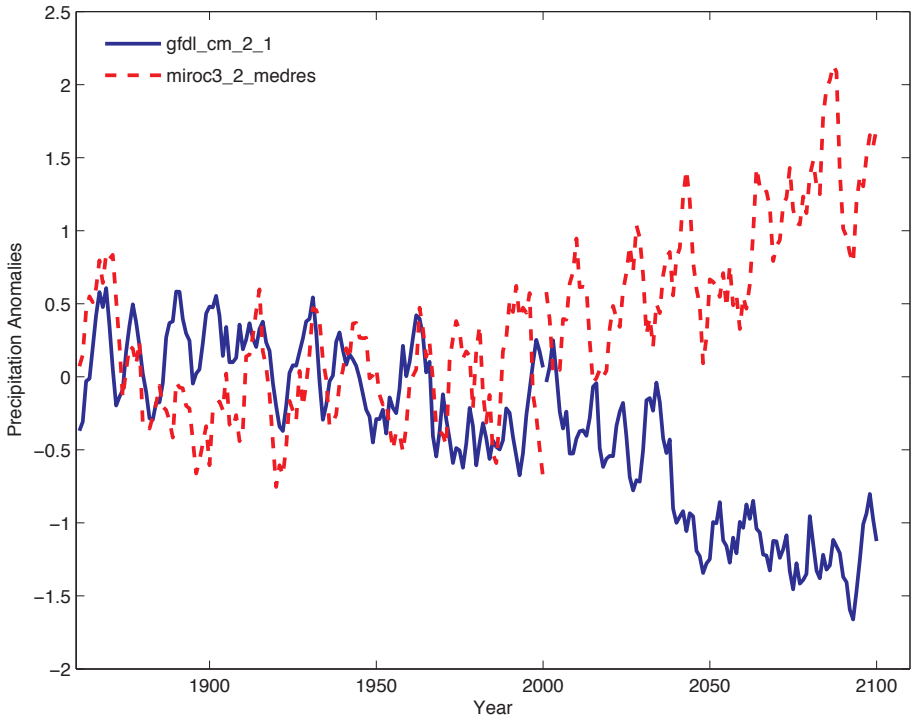

Figure 1. The Sahel rainfall index during the 20$^{\text{th}}$ and 21$^{\text{st}}$ centuries, as simulated by the GFDL (solid line) and MIROC (dashed line) models. Anomalies are in millimeters per day.

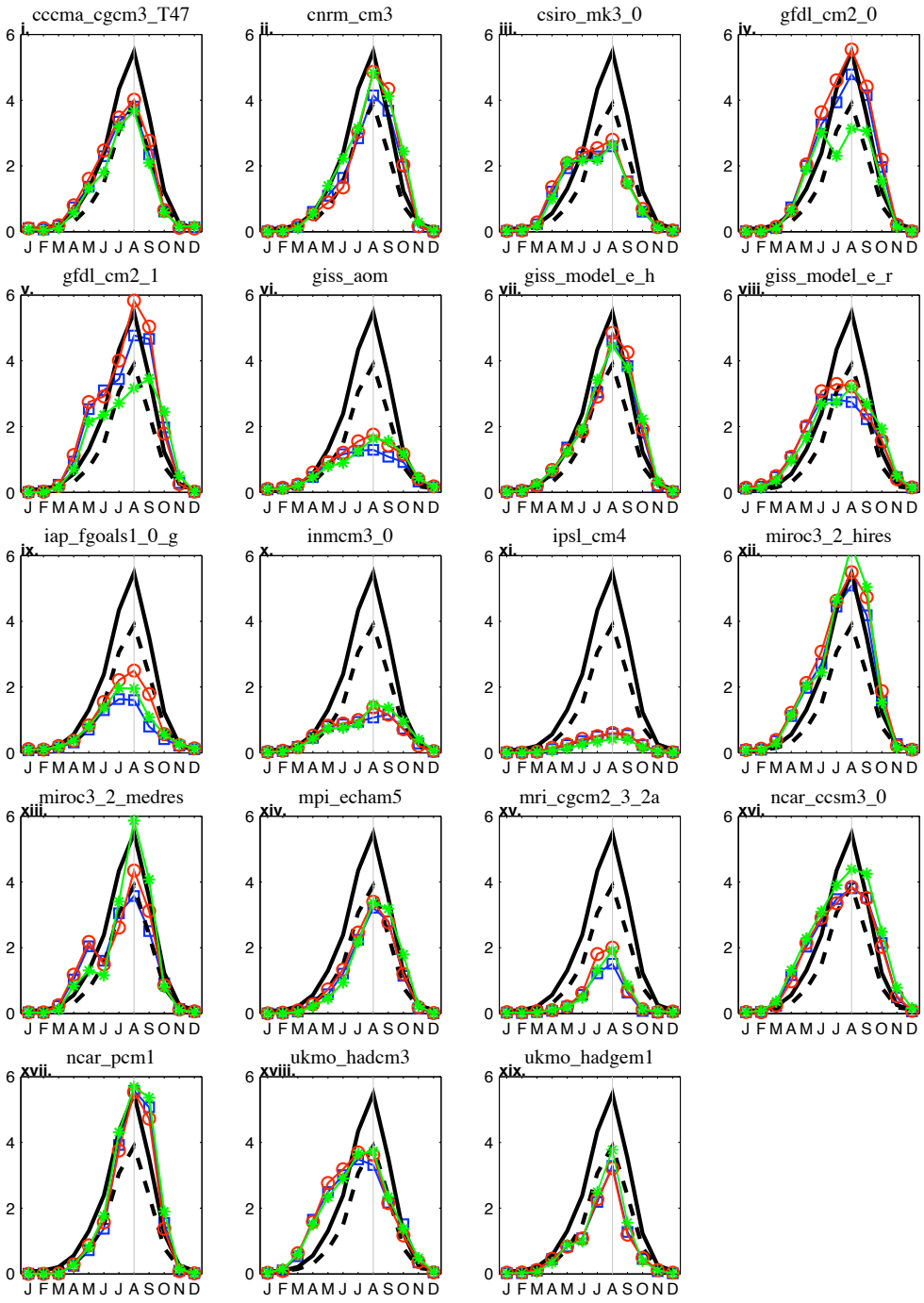

Figure 2. Annual cycle of Sahel precipitation (in mm day^{-1}) in observations (the solid black curve is the mean climatology in the Hulme dataset, the dashed black curve is CMAP) and in simulation of the pre-industrial epoch (PI, red circles), the 20th century (XX, blue squares), and the 21st century (A1B, green asterisks).

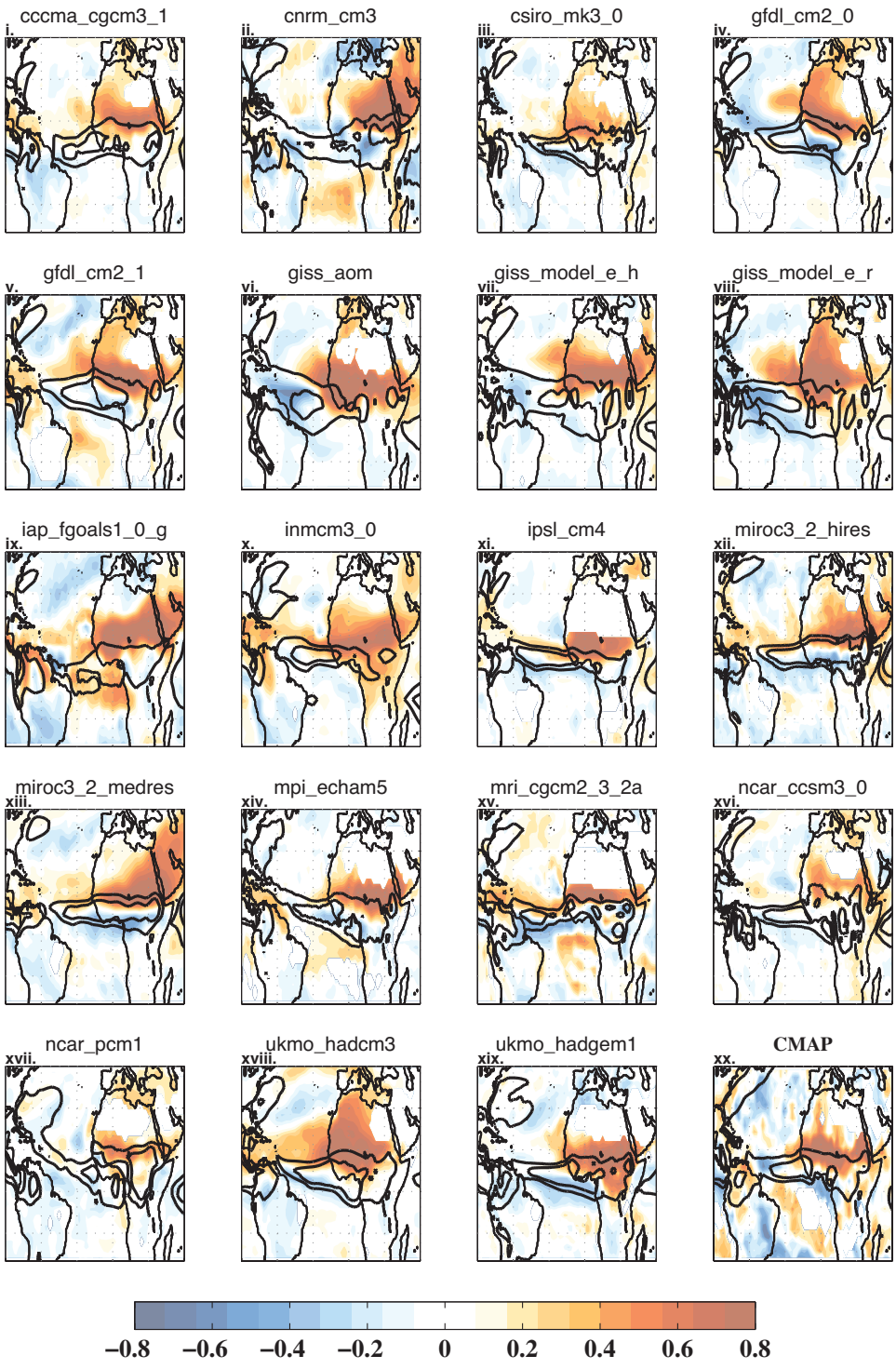

Figure 3. Contours: 4 and 8 mm/day contours of JAS precipitation. Shading: Correlation between the Sahel index and JAS rainfall. Warm colors indicate positive correlations, cold colors negative correlations, the shading interval is .08

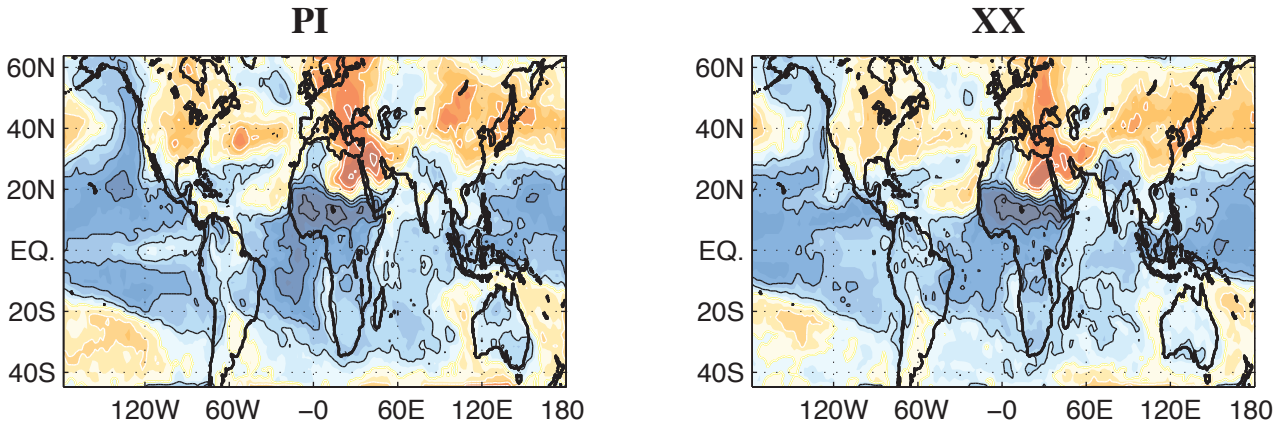

Figure 4. Percentage of models showing positive (dark grays / warm colors shading, white contours) or negative (light grays / cool colors shading, black contour) significant correlations between the Sahel index and surface temperature at each gridpoint. The left panel is for the PI detrended simulations, the right panel for the XX detrended simulations. The contour interval is 20%, the shading interval 40% (black and white version) or 10% (color version). See text for further details.

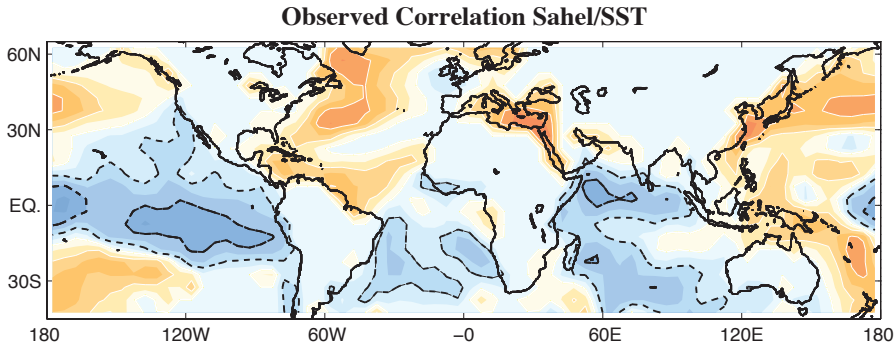

Figure 5. Observed positive (dark grays / warm colors shading, white contours) or negative (light grays / cool colors shading, black contour) correlations between the Sahel index (Hulme data set) and sea surface temperature (Kaplan data set) at each gridpoint. The contour interval is 0.20, the shading interval 0.4 (black and white version) or 0.1 (color version).

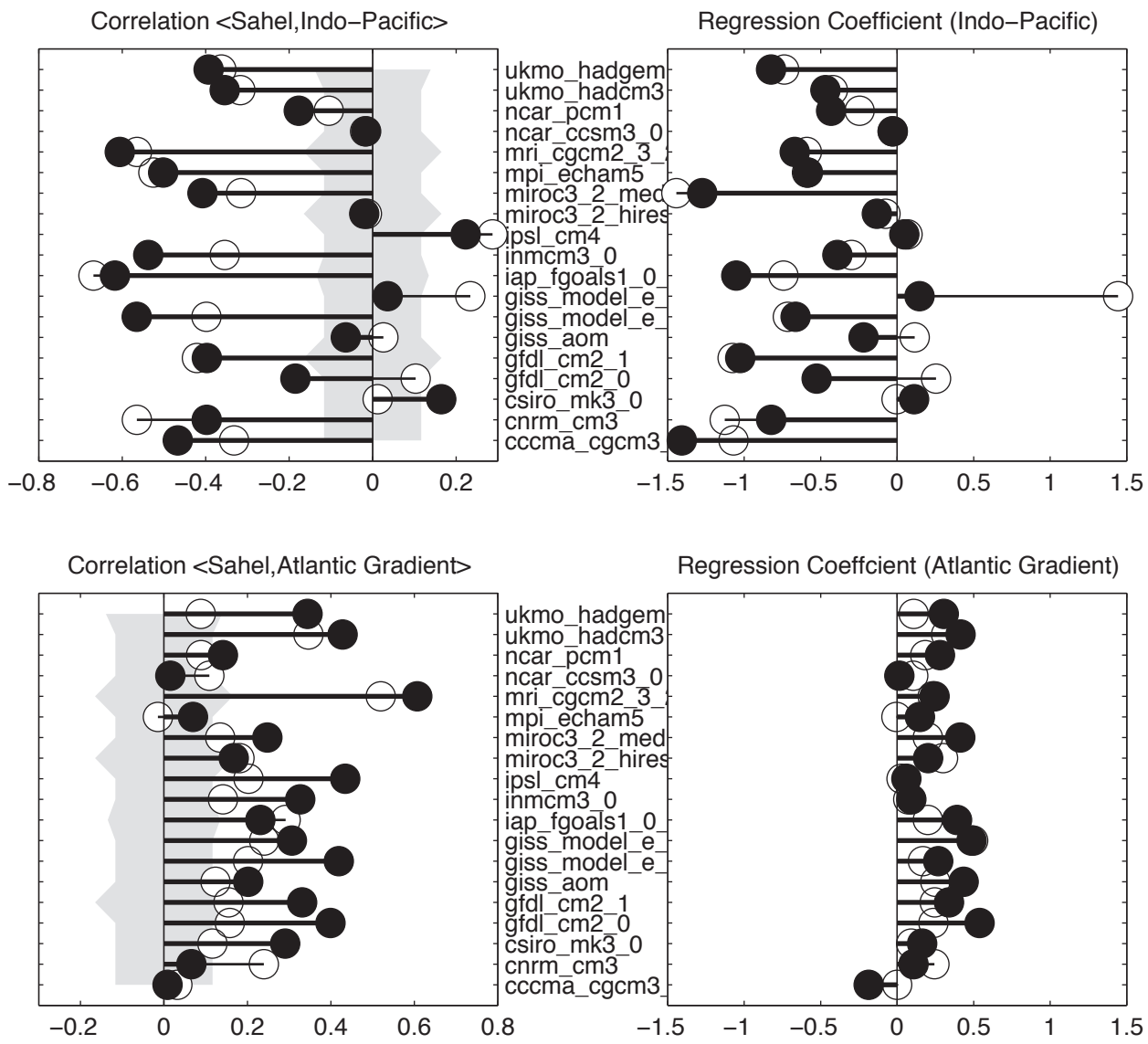

Figure 6. Pre-industrial correlations (left) and regression coefficients (right) between the Sahel index and (top) the area averaged Indo-Pacific SST and (bottom) the difference of north tropical Atlantic and south tropical Atlantic SST. Open circles are for timeseries that have been detrended; filled circles for detrended and 5-year running mean timeseries.

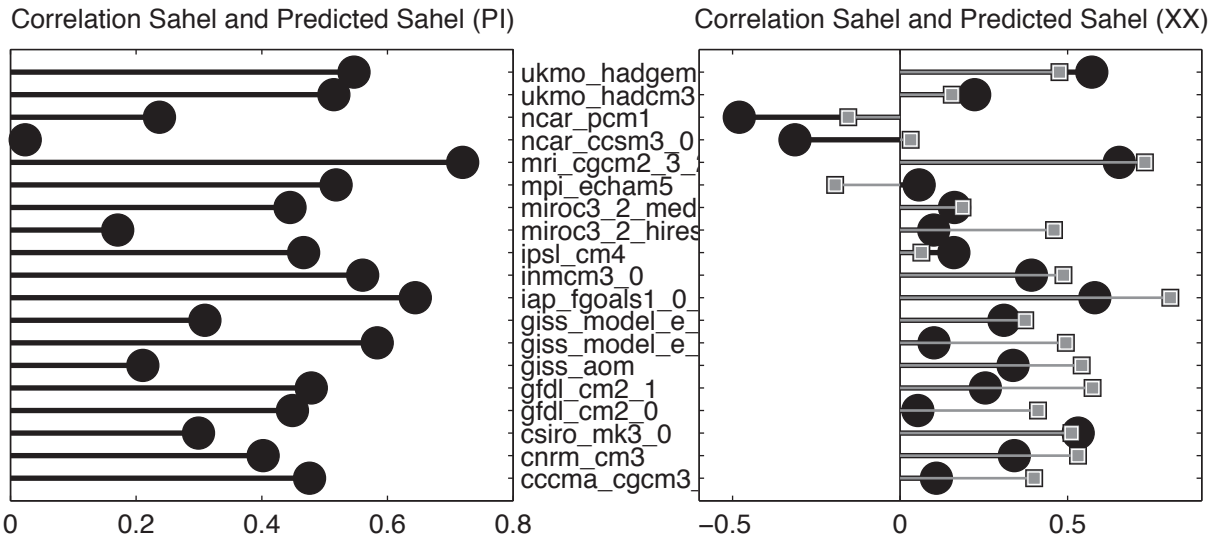

Figure 7. Correlations between simulated and linearly predicted Sahel index in the (left) PI and (right) XX integrations. The coefficients of the linear model come from the JAS, detrended, 5 year running mean time series of Sahel rainfall, Indo-Pacific SST and Atlantic SST gradient in the PI integrations. All timeseries have been subjected to a 5-yr running mean; dots refer to detrended timeseries, squares to timeseries retaining the trend.

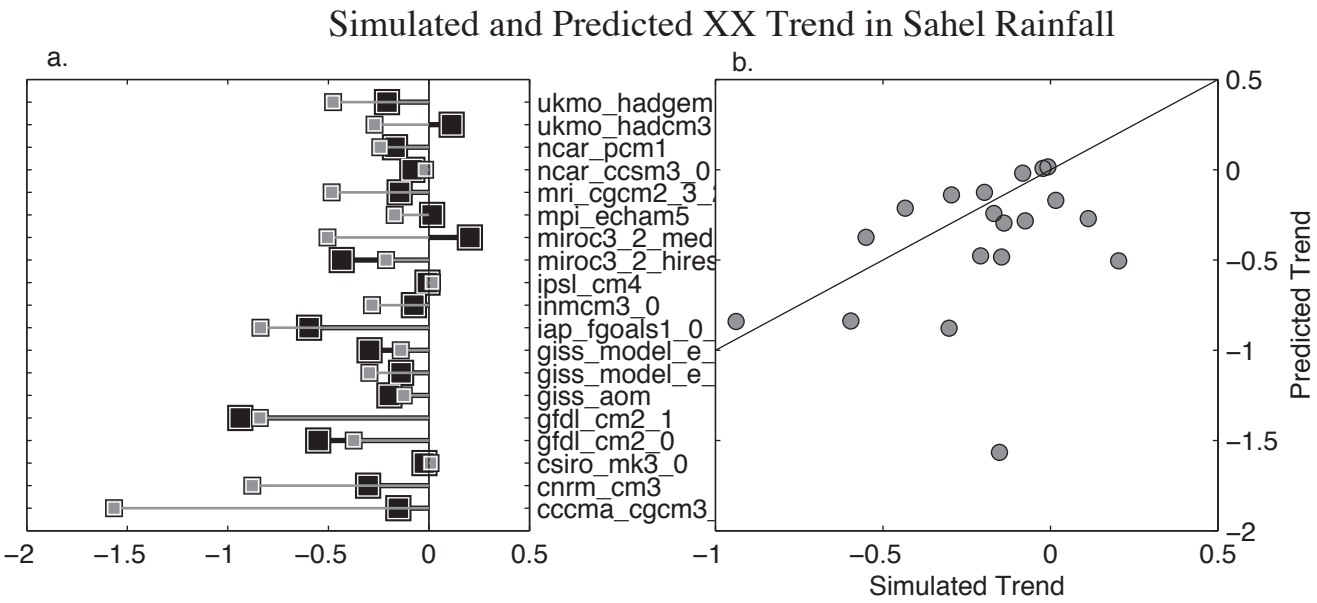

Figure 8. (a.) Linear trends in the simulated XX Sahel rainfall (large squares) and the predicted Sahel timeseries obtained by linear regression from the simulated XX SST (small squares). The linear regression model was trained on the detrended, 5-yr running means of the PI simulations. The trends are calculated over the length of the entire XX simulations, which might cover different periods for different models. (b.) Scatter plot of the simulated and predicted trends shown in panel (a.).

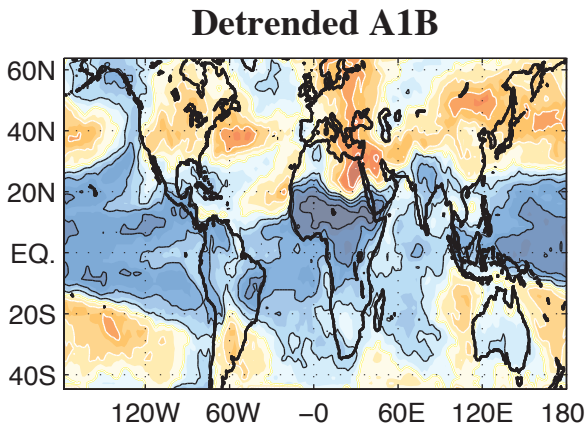

Figure 9. As in Figure 4 but for the A1B simulations.

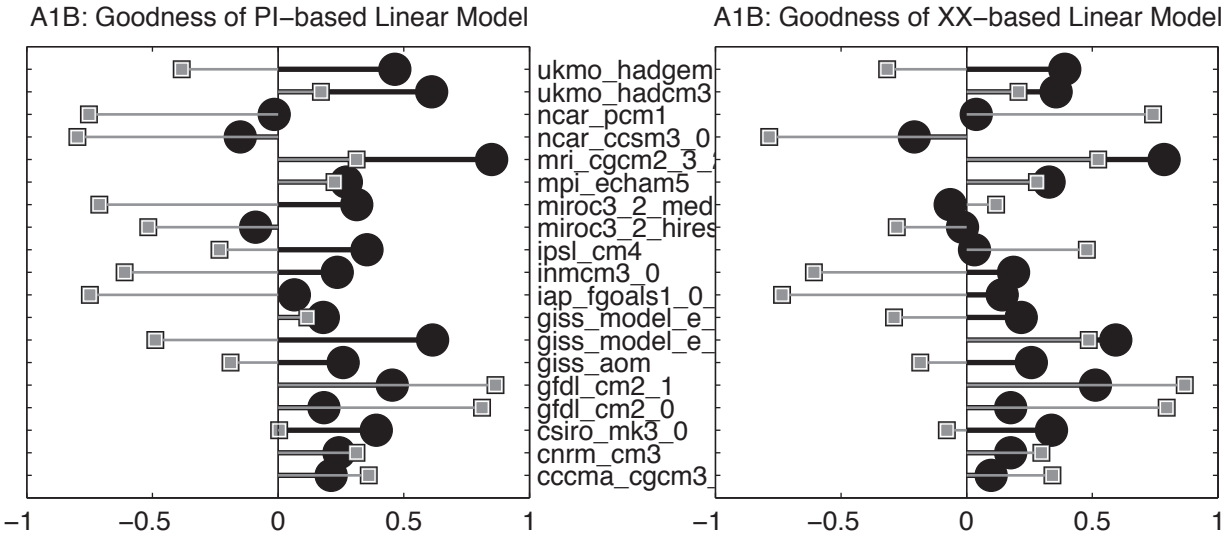

Figure 10. Correlations between simulated and linearly predicted Sahel index in the A1B integrations. The coefficients of the linear model come from the JAS, 5 year running mean time series of Sahel rainfall, Indo-Pacific SST and Atlantic SST gradient in the (left) detrended PI and (right) XX integrations. All A1B timeseries have been subjected to a 5-yr running mean; dots refer to A1B detrended timeseries, squares to A1B timeseries retaining the trend.

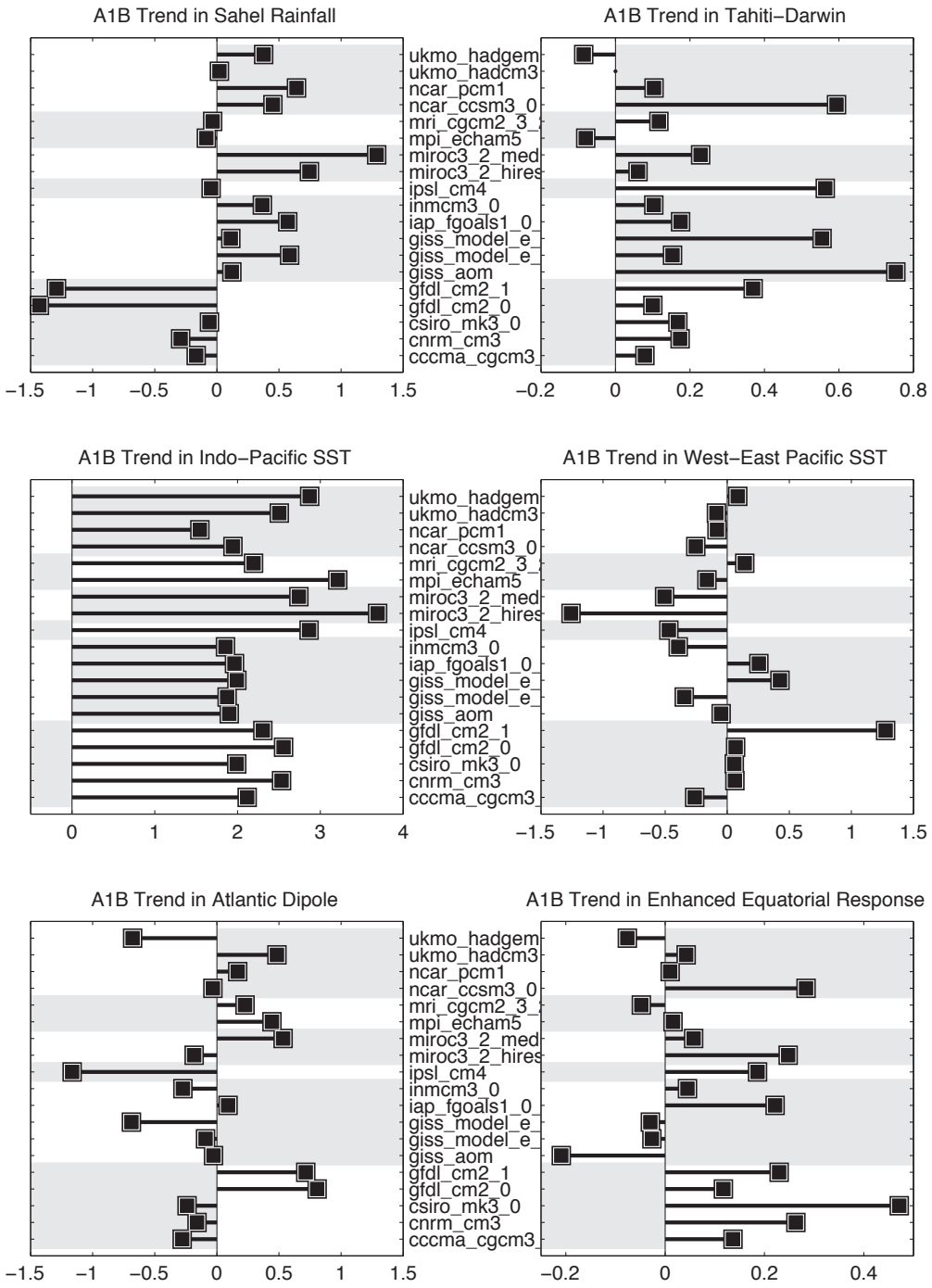

Figure 11. Linear trends over the years 2000-2100 in the A1B integrations in (top left) Sahel index, (middle left) Indo-Pacific SST, (bottom left) Atlantic SST meridional gradient, (top right) Tahiti-Darwin sea level pressure difference, (middle right) west equatorial Pacific - east equatorial Pacific SST difference, and (bottom right) the enhanced equatorial response index (Liu et al., 2005).

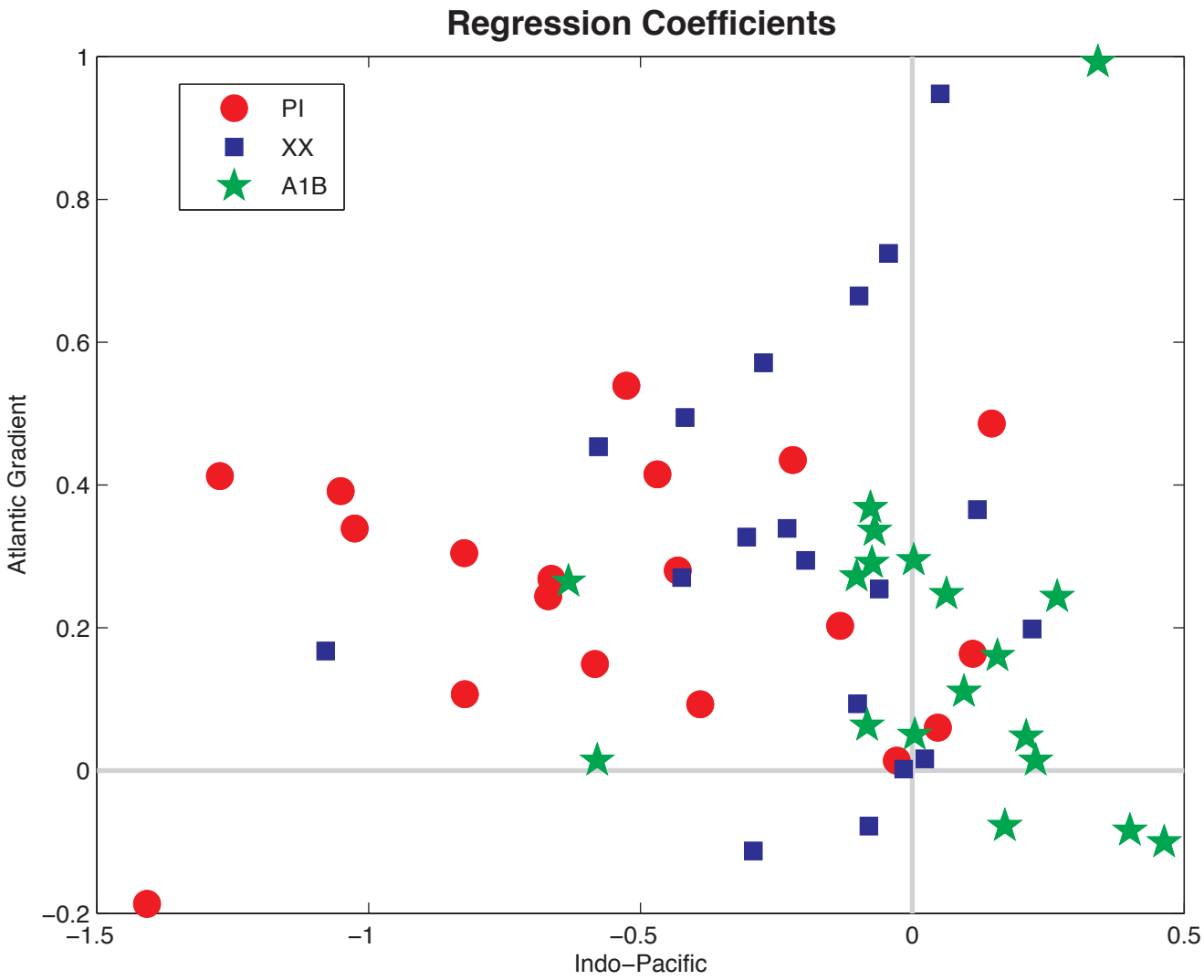

Figure 12. Scatter plot of the bi-variate linear model regression coefficients between the Sahel index and the Indo-Pacific SST and Atlantic SST meridional gradient. Red dots are for the PI integrations, blue squares are for XX and green stars are for A1B.

Tables

Table 1. Model name; Resolution of the atmospheric and oceanic component models (in degrees); Start date for the XX run; forcings used in the XX integrations, besides the increasing well-mixed greenhouse gases and the direct effect of sulfate aerosols (Natural forcings are solar output and volcanic emissions; Land refers to land use changes; OC is organic carbon, BC is black carbon, IE is the indirect effect of sulfate aerosols); Length of PI run (note that for most analyses we have used 200-year-long records, except for the high resolution MIROC model).

Model	Atmos.Res.	OceanRes.	XXStartDate	Additional20thCenturyForcings					LengthPI
				Natural	Land	OC	BC	IE	
ccma_cgcm3	3.75 x 3.71	1.85 x 1.85	1850	N	N	N	N	N	500
cnrm_cm3	2.81 x 2.79	2 x 0.5	1860	N	N	N	N	N	500
csiro_mk3_0	1.88 x 1.87	1.88 x 0.84	1871	N	N	N	N	N	380
gfdl_cm2_0	2.5 x 2	1 x 1/3	1861	Y	Y	Y	Y	N	500
gfdl_cm2_1	2.5 x 2	1 x 1/3	1861	Y	Y	Y	Y	N	500
giss_aom	4 x 3	4 x 3	1850	N	N	N	N	N	250
giss_model_e_h	5 x 4	2 x 2	1880	Y	Y	Y	Y	Y	400
giss_model_e_r	5 x 4	5 x 4	1880	Y	Y	Y	Y	Y	500
iap_fgoals1_0_g	2.81 x 3.05	1 x 1	1850	N	N	N	N	N	200
inmcm3_0	5 x 4	2.5 x 2	1871	Y	N	N	N	N	330
ipsl_cm4	3.75 x 2.54	2 x 1	1860	N	N	N	N	N	320
miroc3_2_hires	1.13 x 1.12	0.28 x 0.19	1900	Y	Y	Y	Y	Y	100
miroc3_2_medres	2.81 x 2.79	1.4 x 0.5	1850	Y	Y	Y	Y	Y	500
mpi_echam5	1.88 x 1.87	1.5 x 1.5	1860	N	N	N	N	Y	505
mri_cgcm2_3_2a	2.81 x 2.79	2.5 x 0.5	1851	Y	N	N	N	N	350
ncar_cccsm3_0	1.41 x 1.40	1.13 x 0.27	1870	Y	N	N	Y	N	500
ncar_pcm1	2.81 x 2.79	1.13 x 0.27	1890	Y	N	N	N	N	350
ukmo_hadcm3	3.75 x 2.50	1.25 x 1.25	1860	N	N	N	N	Y	341
ukmo_hadgem1	1.88 x 1.25	1 x 1/3	1860	N	N	Y	Y	Y	230